Role of stable eigenmodes in gyrokinetic models of ion temperature gradient turbulence

D. R. Hatch,[1] P. W. Terry,[1] W. M. Nevins,[2] and W. Dorland[3]

[1]*University of Wisconsin-Madison, Madison, Wisconsin 53706, USA*
[2]*Lawrence Livermore National Laboratory, Livermore, California 94551–0808, USA*
[3]*University of Maryland, College Park, Maryland 20742, USA*

Investigation of ion temperature gradient turbulence in gyrokinetic models shows that some of the key features of reduced models associated with saturation by nonlinearly excited damped eigenmodes carry over to gyrokinetics. For nonzonal wavenumbers the frequency spectrum in gyrokinetics is broader by a factor of 10 than simple nonlinear broadening of the most unstable eigenmode. The width, including its variations with wavenumber and temperature gradient scale length, closely tracks accessible stable eigenmodes as approximated by a gyro-Landau fluid model for the same parameters. Cross-phase probability distribution functions (pdfs) and fluxes show nonlinear behavior consistent with stable eigenmodes in nonzonal wavenumbers contributing to 30% of the fluctuation energy. Phase pdfs and cross-phase time histories show that multiple eigenmodes [in addition to high frequency geodesic acoustic modes (GAMs)] are a significant part of the $k_y=0$ spectrum. Two possible roles of zonal modes in saturation are proposed. First, known nonlinearly accessible stable zonal eigenmodes (in addition to zonal flows and GAMs) are discussed and it is suggested that if these eigenmodes are excited they may be the primary arbiter of saturation. Second, zonal modes may facilitate energy transfer from unstable eigenmodes to stable eigenmodes at finite k_y. © *2009 American Institute of Physics*. [DOI: 10.1063/1.3079779]

I. INTRODUCTION

Plasma microinstabilities that saturate by spectral transfer can do so through either of two channels. In one, the eigenmode of the instability, which uniquely characterizes the fluctuation structure in the linear growth phase, remains in force as energy is transferred to small wavelength. There, the growth rate of the unstable eigenmode turns negative because of dissipative processes, and the energy carried by the cascade is removed from the spectrum. In the other, the nonlinearity transfers energy to stable-eigenmode branches whose damping saturates the instability. This can occur even at the same wavenumbers at which the instability is driving the turbulence. Two well known stable eigenmodes are zonal flows and geodesic acoustic modes (GAMs). The role of zonal flows in saturating turbulence has been extensively studied and is most often explained as a shearing process rather than a direct energy sink (in the absence of collisional damping). In this paper we are concerned with excitation of other damped eigenmodes both at zonal ($k_y=0$) and nonzonal ($k_y \neq 0$) wavenumbers and their role as direct energy sinks in saturation. These often neglected stable eigenmodes are roots of the linear dielectric. Their growth rate is zero or negative for all wavenumbers. When stable eigenmodes are excited to finite amplitude the fluctuation structure of the unstable eigenmode is nonlinearly mixed with that of stable eigenmodes at each wavenumber, producing a nonlinear eigenmode. These two saturation outlets can be represented as manifolds, with one for each eigenmode of the dielectric. Figure 1 represents the manifolds as planes of two-dimensional (2D) wavenumber space and depicts a situation in which there is one unstable eigenmode and one stable eigenmode. Energy transfer between regions of positive and negative growth rates in the unstable manifold is usually a cascade, connoting a process with multiple steps. Transfer between manifolds can access damped wavenumbers in a single step. Despite the direct nature of this channel, a survey of theoretical work on saturation shows that damped eigenmodes have not been treated as saturation-producing energy sinks,[1] except in a few cases.[2,3]

Valid numerical solutions of the dynamical equations capture both saturation mechanisms. However, which mechanism dominates makes a large difference in how the turbulence is understood conceptually, in how important quantities are estimated, and significantly, in the approximations used in numerical and analytical calculations. For example, if saturation involves only the unstable manifold, the rate of growth or damping at wavenumber k can be calculated using linear theory. If saturation involves stable manifolds, growth and damping are intrinsically nonlinear, i.e., they depend on the level of each stable eigenmode. Moreover, if energy transfer to damped eigenmodes is a significant saturation mechanism, these modes must be properly resolved in numerical modeling, and their physics must be accurately represented. Approximations such as mixing length rules and quasilinear fluxes implicitly assume that stable manifolds are unimportant in saturation.

Recent work has shown that stable eigenmodes saturate trapped electron mode (TEM) turbulence and ion temperature gradient (ITG) turbulence in reduced, local 2D fluid models.[2,3] These models allow calculation of a complete fluctuation basis set from the linear eigenmodes. Projection of initial value evolution onto this basis shows that the
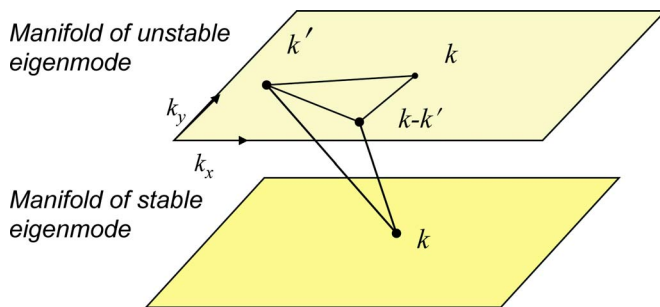
FIG. 1. (Color online) Diagram representing two saturation mechanisms: (1) Spectral transfer to high-k dissipative wavenumbers, represented by the upper plane, and (2) nonlinear transfer to damped linear eigenmodes, represented by the lower plane.

stable-eigenmode fluctuations initially decay with their linear damping rate until reaching a threshold, after which they grow exponentially through direct mode coupling with fluctuations on the unstable manifold (as depicted in Fig. 1).[2] At finite amplitude they radically change dissipation, spectra, transport fluxes, and statistics.[2–5] It is important to know to what extent this behavior carries over to other systems, including those with comprehensive models. Following the prescription of Refs. 2 and 3 it is possible to determine which stable eigenmodes are excited and what role they play in saturation energetics for other fluid systems. Efforts in this regard are underway.[6] In kinetic theory the zeros of the dielectric must be determined, of which there may be an infinite number, and these roots must be incorporated into saturation analyses. In gyrokinetic computation the issue of stable-eigenmode dynamics is complicated by an emphasis on initial value computation at the expense of solving eigenmodes.

Stable-eigenmode roots of the linearized gyrokinetic equations are nevertheless being identified. The most familiar of these are zonal flows and GAMs.[7,8] New classes of eigenmodes, especially at $k_y=0$, are being found.[9] Zonal flows have been studied the most extensively.[10] Because they are essentially undamped[11] in the absence of collisions, zonal flows are ineffective as finite-amplitude-induced energy sinks in collisionless regimes like those in this study. In simulations with finite collisionality, it has been shown that collisional damping of zonal flows can strongly regulate fluctuation amplitude and transport.[12] Zonal flows are most often thought to affect saturation through their shearing.[13] Shearing is a process that enhances the transfer to short wavelength damped fluctuations.[14] In terms of the manifold picture of Fig. 1, zonal flows represent a second manifold with no damping that acts as a catalyst to move energy on the first manifold to short dissipated wavelengths. However, this mechanism is less effective than commonly believed. Zonal flows are driven by nonlinear mode coupling; hence their shearing rate is comparable to instability growth rates, a feature observed in both experiment and simulation.[15,16] Most theoretical treatments of shear suppression indicate that shearing rates comparable to growth rates yield a moderate amplitude reduction, not a reduction of an order of magnitude or more, see Refs. 17 and 18. Instead, our interest here

is with damped eigenmodes that represent a potentially significant *sink* of fluctuation energy at both zonal and nonzonal wavenumbers. In the local 2D fluid models saturation is caused by stable eigenmodes that are neither zonal flows nor GAMs, although a region of their manifolds contains zonal wavenumbers ($k_y=0$). In these systems the anisotropy of the drift frequency enhances spectral transfer to $k_y=0$.[19,20] Any damped eigenmode that takes up this energy will provide a saturation sink, whether it is a GAM or something else. In this regard it is important to maintain a distinction between zonal flows and zonal wavenumbers (i.e., $k_y=0$). Zonal flows satisfy $k_y=0$, but so do other eigenmodes for that part of the spectrum. Spectral properties associated with $k_y=0$ thus involve a combination of zonal flows and other eigenmodes. If the latter are damped they can saturate instability in a way that zonal flows cannot.

This paper investigates whether stable eigenmodes are involved in the saturation of ITG turbulence as modeled by GYRO.[21] This is a difficult question and the results presented here represent an initial effort. The primary difficulty is that GYRO is an initial value code. It is possible to determine only the growth rate of the fastest growing unstable eigenmode (from amplitude e-folding in the linear instability phase). This calculation yields no information about other eigenmodes. The gyrokinetic code, GENE,[22,23] is equipped with an eigenmode solver[24] which can resolve the full spectrum of unstable and stable eigenmodes and future work is planned to utilize this capability to verify and expand the results presented here. However, this work is limited to initial value gyrokinetic solvers and as a result we develop other less direct methods of establishing the presence of stable eigenmodes in saturation. To compensate for diagnostic limitations these methods utilize benchmarked cases for comparison with other comprehensive solvers. Limitations and uncertainties make it important to develop multiple tests for inferring stable-eigenmode activity.

We examine three tests of stable-eigenmode activity applied to fluctuations in the saturated state. All gyrokinetic simulations used for this study employ flux tube geometry. Fluctuation data are taken at the outboard midplane and thus are a function of radial (k_x) and binormal (k_y) wavenumbers. The first test involves analysis of the width of the frequency spectrum in saturation. The width is compared to that expected if only the most unstable eigenmode is present and to linear frequency spreads determined by solving for the eigenmodes of the fluid equations of GLF23.[25] This analysis is applied to the CYCLONE (Ref. 26) base case for which it is established that the growth rates of GLF23 and GYRO are in close agreement. The second test involves statistical and time history analysis of phase angles in the cross correlation of potential and internal energies. Like the first test, this looks at the spread of angle away from that of the fastest growing eigenmode and considers how much spread is required to implicate stable eigenmodes. The third test involves comparisons of the quasilinear and nonlinear heat fluxes. It looks for a systematic reduction of the nonlinear flux relative to the quasilinear approximation, indicating a nonlinear state that mixes the unstable eigenmode with stable eigenmodes. For the diagonal flux element, stable eigenmodes give a negative

contribution to the flux and therefore reduce it relative to the quasilinear value. All three tests give evidence that stable eigenmodes are excited in GYRO. To inform the search for stable-eigenmode activity in GYRO we briefly review the results of the reduced ITG model where stable eigenmodes are observed directly.

Two of these tests are also applied to fluctuations at zonal wavenumbers. In addition to GAMs, there is evidence that other eigenmodes are active at $k_y=0$. These eigenmodes may be robustly damped for zonal wavenumbers where spectral power peaks. These wavenumbers also show the strongest modifications to cross correlations. These measurements lead to speculation regarding the role of zonal modes in relation to damped eigenmodes. Because of the high fluctuation intensity at zonal wavenumbers, it is plausible that damped zonal eigenmodes play a key role in saturation as a direct energy sink. In addition, it is also possible that zonal modes are catalysts for driving damped mode excitation at nonzero binormal wavenumbers. This is the topic of current research. This paper is organized as follows. Section II briefly describes stable-eigenmode physics in the reduced ITG model as it relates to tests described herein and tests that might be carried out later. These tests are applied to nonzonal wavenumbers in Sec. III, with subsections on the frequency spectrum, transport fluxes, and phase probability distribution functions (pdfs). Stable eigenmodes in zonal wavenumbers are examined in Sec. IV. This section emphasizes phase pdfs and cross correlation evolution. Conclusions are given in Sec. V.

II. STABLE EIGENMODES IN A LOCAL FLUID MODEL

To help interpret GYRO results, we review stable-eigenmode effects in a reduced system where stable eigenmodes can be exactly calculated and observed directly. The following results, which we only summarize in this paper, are presented in detail in Ref. 3. The reduced system is based on a fluid model for the slablike branch of ITG with equations for vorticity, ion pressure, and parallel ion flow.[27] In the local limit where the parallel wavenumber $k_\parallel$ is taken to be constant the model retains a slab-ITG-like linear growth rate that is proportional to $[k_\parallel^2(1+\eta_i)/\tau]^{2/3}$, where η_i is the ratio of density gradient to temperature gradient scale length and $\tau=T_e/T_i$.[3] While this model is very simple compared to comprehensive models, its nonlinearities are similar and include $E \times B$ advection of vorticity, pressure, and parallel flow. This system does not have a zonal flow but does have a marginally stable eigenmode with zonal and nonzonal wavenumbers. There is also a damped eigenmode that nearly forms a complex conjugate pair with the unstable eigenmode.

With three fields (pressure, parallel flow, and potential, with vorticity as the Laplacian of the potential) the three linear eigenmodes can be solved directly from the linearized equations of motion. Because the linear eigenmodes form a complete basis, the original evolution equations can be transformed to the basis of the linear eigenmodes, yielding dynamical equations for the amplitude of each eigenmode. We denote each amplitude by β_j with $j=1$, 2, or 3. The evolution equations in the eigenmode basis are diagonal in the linear coupling, by construction, while each amplitude is driven nonlinearly by a linear combination of the three nonlinearities of flow, pressure, and vorticity advection. Because each field is a linear combination of the three eigenmodes, the nonlinearities have quadratic couplings of each eigenmode with itself and with each of the other two eigenmodes. In Fourier space these couplings involve the products $\beta_i(k')\beta_j(k-k')$. Let the linearly unstable eigenmode be β_1. During the linear growth phase when $\beta_1 \sim \exp(\gamma t)$, terms proportional to $\beta_1(k')\beta_1(k-k')$ in the nonlinearities of the β_2 and β_3 equations drive exponential growth at effectively twice the linear growth rate. In evolution from an infinitesimal initial state this nonlinear exponential growth dominates as soon as the nonlinear terms are large enough to exceed the exponentially decaying initial value transient.[4]

The nonlinear growth of a stable eigenmode saturates at a level determined from the balance of net transfer into the eigenmode and its linear damping. If the mode is marginal, its amplitude is set by a balance of nonlinear terms. A damped eigenmode has a noticeable effect on instability-driven turbulence if it produces a noticeable drain on the unstable eigenmode. This occurs if the rate of transfer from unstable to stable manifolds is comparable to the rate of transfer within the unstable manifold.[3] For the reduced model, both stable eigenmodes have a noticeable effect according to this criterion. The following is essential behavior observed from numerical solutions of the initial value problem that reveals the presence of stable eigenmodes at a level sufficient to affect saturation.

(1) Amplitude evolution and frequency spectrum: In the reduced model both the spectral transfer rates involving stable eigenmodes and the stable-eigenmode saturation amplitudes are comparable to those of unstable eigenmodes. In fluid models the complete basis set of eigenmodes provides a unique decomposition of the original fields into eigenmodes for observation. This is the way in which eigenmode amplitudes are tracked in Fig. 2 of Ref. 3. If knowledge of the complete basis is not available other unique observables must be sought. The wavenumber spectrum of itself is not such an observable. A shift of the peak away from the wavenumber of the most unstable eigenmode represents a significant transfer of energy away from that wavenumber but does in general reveal whether the wavenumbers of the new peak are on the unstable or stable manifolds. A better spectrum observable is the frequency spectrum at fixed wavenumber. In the linear growth phase when amplitudes are dominated by the unstable eigenmode, a unique frequency associated with the instability can be derived from simulation data. If stable eigenmodes are insignificant in saturation, the frequency spectrum will peak at this mode frequency, with a finite width governed by nonlinear transfer rates. Nonlinear transfer rates must be comparable to the linear growth rate to balance the instability. If the peak spreads significantly beyond this width, stable eigenmodes are implicated. If there is information about the frequencies of stable eigenmodes, these can be marked on the spectrum and

energy at that frequency can be ascribed to that eigenmode provided it is the only eigenmode at that frequency, and other eigenmodes are separated by more than the nonlinear spread.

(2) Transport flux: If stable eigenmodes at nonzonal wavenumbers are a significant energy sink for saturation, transport fluxes will deviate from the quasilinear values. If the transport matrix is primarily diagonal, the damped eigenmodes will drive inward fluxes, reducing the overall flux from the quasilinear value. For the reduced model this is evident in Fig. 2 of Ref. 3. The flux is very bursty but remains lower than the quasilinear value both during and between bursts. Because the temperature and density gradients are fixed in this model, the burstiness is associated with long time sloshing between the eigenmodes. Therefore, there are times when the flux is quite close to the quasilinear value and times when it is quite far. If damped eigenmodes at zonal wavenumbers play a significant role in saturation, then the magnitude of the net impact of damped eigenmodes will be underestimated by tests that apply solely to nonzonal wavenumbers, such as the comparison of quasilinear and nonlinear fluxes. This is because zonal wavenumbers make no contribution to anomalous transport fluxes associated with nonlinear $E \times B$ advection. Since spectral transfer to zonal wavenumbers of damped eigenmodes is generally enhanced over transfer to other wavenumbers in systems with drift frequencies,[4] the difference between true and quasilinear fluxes will significantly underestimate the effect of damped eigenmodes.

(3) Cross phases: The cross correlations between fluctuating fields are complex valued. Because eigenmodes specify a unique complex proportionality between Fourier amplitudes of different fields, the angle in the complex plane of each cross correlation assumes a unique value for each eigenmode. If the unstable eigenmode dominates saturation, a pdf of the angle should be close to a delta function at the angle of the unstable eigenmode. The time history should show small fluctuations about this angle. If the pdf is broadened, the cross phase assumes other values and reflects the presence of eigenmodes other than the most unstable mode. In the reduced model the cross phase evolves intermittently as seen in Fig. 4 of Ref. 3. There are periods when the cross phase fluctuates about a fixed angle that is not the angle of the unstable eigenmode and periods when it rotates through a range of values.

(4) Nonlinear growth rate: A direct but less familiar measure of stable-eigenmode effects on saturation is the nonlinear growth rate.[2,3] This measures the rate at which energy is extracted from gradient free energy sources and fed into the fluctuations. This is a measure of a fundamentally dissipative process, unlike spectral energy transfer, which is generally conservative. At infinitesimal amplitude the nonlinear growth rate asymptotes to the linear growth rate. If this quantity changes at finite amplitude the fastest growing unstable eigenmode no longer reflects the true distribution of sources and sinks responsible for saturating the instability. The presence of damped eigenmodes manifests itself as regions in wavenumber space for which the nonlinear growth rate is smaller than the linear growth rate.

The nonlinear growth rate is ideal for observing stable-eigenmode activity in initial value computations because it can be calculated from time histories without *a priori* knowledge of the eigenmode spectrum. It is given by

$$\gamma^{nl}(k) = \frac{1}{U(k)} \left. \frac{dU(k)}{dt} \right|_{nc}, \tag{1}$$

where $U(k)$ is a spectral energy density constructed from a linear combination of the squares of all fluctuating fields relevant to the nonlinear evolution of the system, and $dU(k)/dt|_{nc}$ is the part of the energy rate of change that is not conserved. The nonconserved energy change is given by

$$\left. \frac{dU(k)}{dt} \right|_{nc} = \sum_i a_i \left[A_i^*(k) \left. \frac{dA_i(k)}{dt} \right|_l + A_i(k) \left. \frac{dA_i^*(k)}{dt} \right|_l \right]. \tag{2}$$

where $A_i(k)$ is the amplitude of a fluctuating field, $dA_i/dt|_l$ represents the linear terms of the amplitude evolution equations, and a_i are the coefficients used in constructing $U(k) = \sum_i a_i A_i^2(k)$. The coefficients a_i must be chosen so that $\sum_k U(k)$ is conserved by the nonlinearities of the system (nonlinear invariance) and γ^{nl} must reduce to the linear growth rate at infinitesimal amplitude. These constraints generally specify a unique linear combination of the component fluctuation energies. In fluid systems $dU(k)/dt$ can be constructed from the appropriate energy moments of the evolution equations. Imposing nonlinear invariance, this reduces to a sum of quadratic correlations associated with free energy and allows γ^{nl} to be calculated from time histories without taking a time derivative. For the reduced ITG model,

$$\gamma_k^{nl} = \frac{k_\parallel \, \mathrm{Im}\langle pu_\parallel^* \rangle + k_y \hat{\eta} \, \mathrm{Im}\langle \phi p^* \rangle}{U(k)} - \gamma_D, \tag{3}$$

where

$$U(k) = [(1 + k^2)|\phi|^2 + |u_\parallel|^2 + |p|^2], \tag{4}$$

$\hat{\eta} = (1 + \eta_i)/\tau$, γ_D is the net dissipation of viscosities and collisional diffusivities, and ϕ, $u_\parallel$, and p are Fourier amplitudes of potential, parallel flow, and pressure.[3] Figure 2 shows γ^{nl} as a function of k_x and k_y computed from a numerical solution of the saturated state in the reduced model. For comparison the linear growth rate is shown alongside. The nonlinear growth rate shows regions of wavenumber space with net energy sinks where linearly there are energy sources. This indicates that in these regions the loss of energy from the damping of the nonlinearly excited damped eigenmode exceeds the linear growth rate. Consequently, stable eigenmodes play a major role in the saturation of the reduced model. The nonlinear growth rate is distinct from a recently developed diagnostic for GYRO based on spectral energy transfer rates.[28] A gyrokinetic diagnostic for γ^{nl} will be an element of future studies. For the present effort we focus on the observables (1)–(3) of the above list.
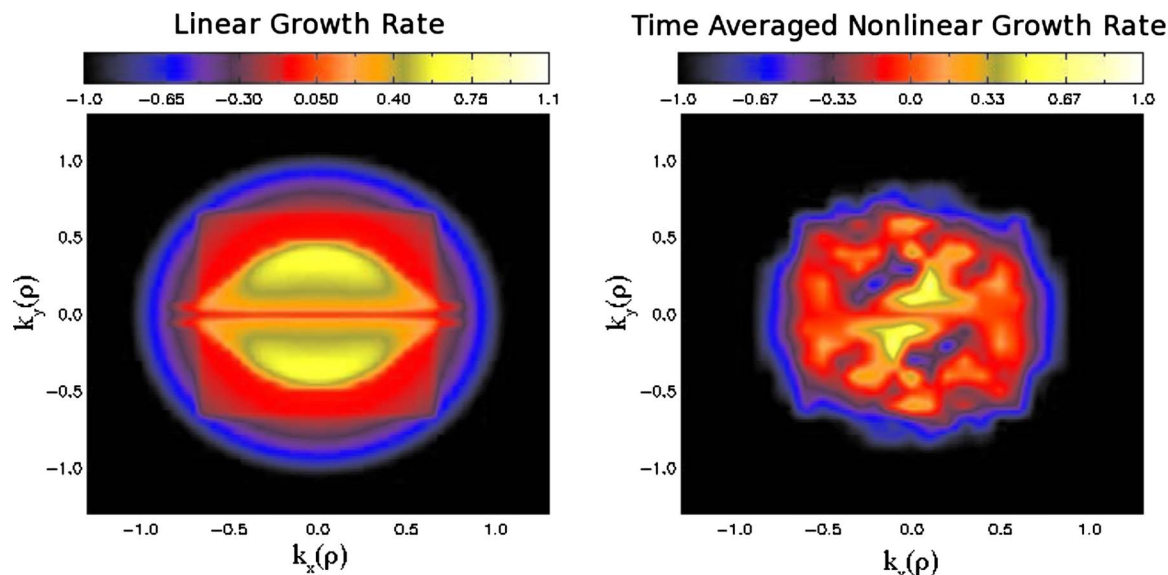
FIG. 2. (Color online) Comparison of linear (left) and nonlinear (right) growth rates from the three-field fluid model simulation. The nonlinear growth rate shows dissipation at wavenumbers that are linearly unstable.

III. NONZONAL WAVENUMBERS

A. Frequency spectra

A linear eigenmode is defined by its frequency (eigenvalue) and its phase relations (eigenvector). If multiple modes are excited to significant amplitudes in a turbulence simulation, one would expect their corresponding mode frequencies to appear in the frequency spectrum. Such is the case with the GAM whose linear mode frequency is readily identified in the nonlinear spectrum. The transport model, GLF23, was used to examine the frequencies and phases of multiple linear eigenmodes. GLF23 is based on an eight-field gyro-Landau fluid model, yielding eight modes. Any fluid representation is a projection of a kinetic equation onto a set of fluid variables, constructed by taking moments of the kinetic equation and making approximations to close the moment hierarchy. Thus, the eight modes accessible to GLF23 should be conceptualized as representative of the modes accessible to the gyrokinetic equation, albeit a finite set. Presumably, if the model is valid, these modes capture most of the turbulent dynamics.

ITG growth rates from GLF23 have been successfully benchmarked against several other models, particularly in standard parameter regimes.[25,29] The GLF23 transport code contains an eigenvalue solver that solves for all eight eigenvalues and eigenvectors. The transport model uses only up to two unstable modes, but there is no reason to dismiss, *a priori*, the stable eigenmodes as being physically relevant. One must be cautious, as the fluid closures break down near poles of the gyrokinetic equation and results with extremely large growth rates should be viewed with skepticism. This is a drawback of any fluid model, and for the parameters examined, spurious modes can seemingly be readily identified and dismissed. In this work, the mode information from GLF23 is used to gain intuition and for qualitative comparison.

For CYCLONE-base case parameters, GLF23 produces the unstable ITG mode and five stable modes whose frequencies cluster around the ITG mode frequency and whose damping rates are on the same order of magnitude as the ITG growth rate. Two other very high frequency (10^5 times larger than the ITG frequency), heavily damped modes were dismissed. It is unlikely that these modes are physical and even if they are, their large damping rates would prohibit them from impacting the dynamics in a significant way.[3]

The linear mode frequencies from GLF23 closely match regions of intensity in the nonlinear frequency spectrum from a corresponding GYRO simulation. In all regions of k space, the frequencies of the five damped modes fall in areas of significant intensity in the nonlinear frequency spectrum as is evident in Fig. 3 (as a function of k_y) and Fig. 4 (as a function of k_x). Figure 3 shows that both the spread in linear mode frequencies and the width of the nonlinear spectrum are roughly proportional to k_y. In addition, the damped mode frequencies seem to be *representative* of the nonlinear spectrum, defining a range of excitation.

Although there is a dearth of theory in the literature regarding frequency spectra, it is commonly believed that the linear growth rate provides an estimate of the expected width of a spectrum.[30] The basic argument is as follows. On average, nonlinear energy transfer must balance the linear energy input due to the instability in order to saturate turbulence. This requirement sets an upper limit on the extent to which nonlinear interactions can modify temporal dynamics and thus broaden a frequency spectrum.

For all wavenumbers examined, the width of the frequency spectrum is much larger than the linear growth rate. This is difficult to explain without invoking the presence of other accessible normal modes with characteristic frequencies represented in the nonlinear spectrum. A scan in temperature gradient scale length L_T was examined in order to
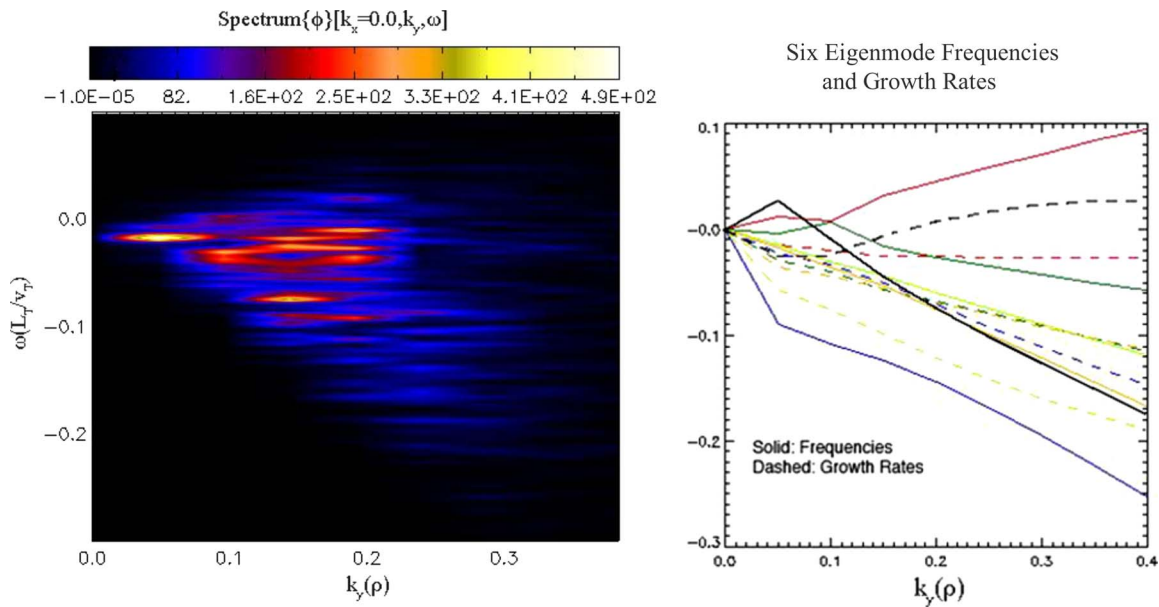
FIG. 3. (Color online) Comparison of the nonlinear frequency spectrum from GYRO simulation data (left) with the frequencies of the ITG mode and five other stable modes (right) as calculated from GLF23 as a function of k_y, plotted on the same plot range. The frequencies of the stable modes closely match regions of intensity in the nonlinear spectrum for a wide range of wavenumbers.

determine the dependence of spectrum width on the linear growth rate. Figure 5 shows the spectra for the wavenumber $k_y=0.2$, $k_x=0$ for a series of L_T values. The central vertical line represents the ITG mode frequency and the solid line on the frequency axis shows the linear growth rate. The spectra for all values of L_T have comparable widths in spite of an increase by a factor of 3 in the growth rate. A corresponding scan of GLF23 runs shows that the width of the spread in damped mode frequencies varies only weakly with L_T and remains close to the widths of the nonlinear spectra. The

width of frequency spectra can also be affected by Doppler shifting due to zonal flows. However, the L_T scan also eliminates Doppler shifting as the primary cause of the width of the spectra since the zonal flow velocity increases strongly with R/L_T as well. Figure 6 shows a plot of the width of the nonlinear frequency spectra in comparison with the spread in damped eigenmode frequencies, linear growth rate, and zonal flow velocity for the wavenumber $k_x=0$ and $k_y=0.2$. The nonlinear spectrum scales well with the spread in damped eigenmode frequencies but does not scale with ei-
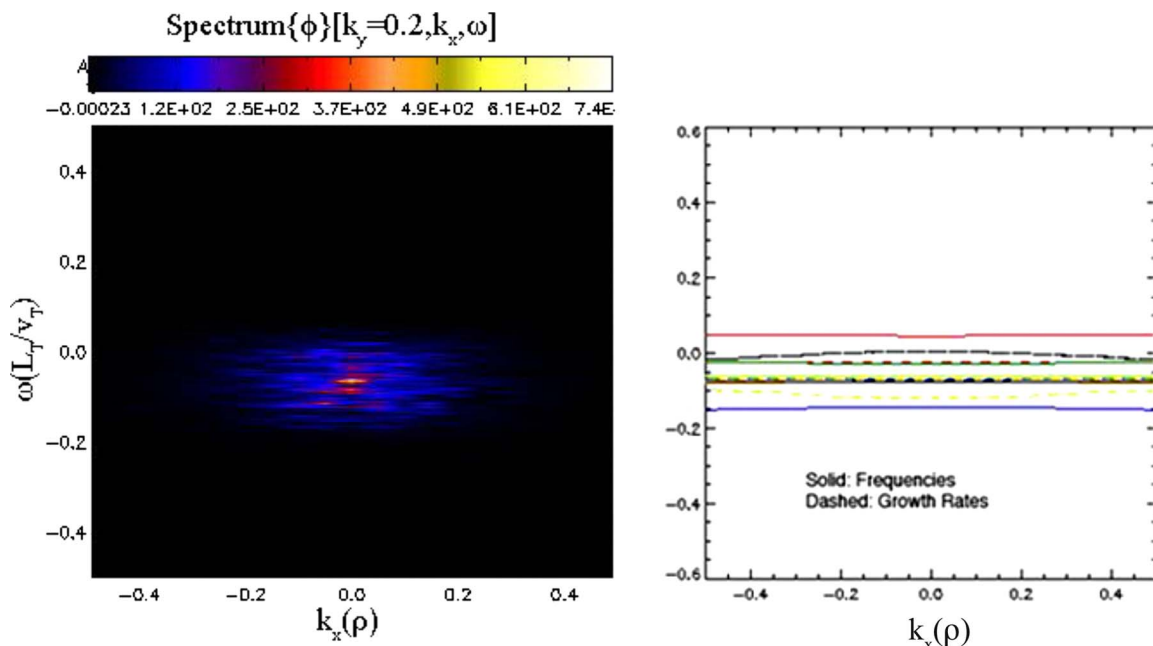
FIG. 4. (Color online) Comparison of the nonlinear frequency spectrum from GYRO simulation data (left) with the frequencies of the ITG mode and five other stable modes (right) as calculated from GLF23 as a function of k_x, plotted on the same plot range. The frequencies of the stable modes closely match regions of intensity in the nonlinear spectrum for a wide range of wavenumbers.
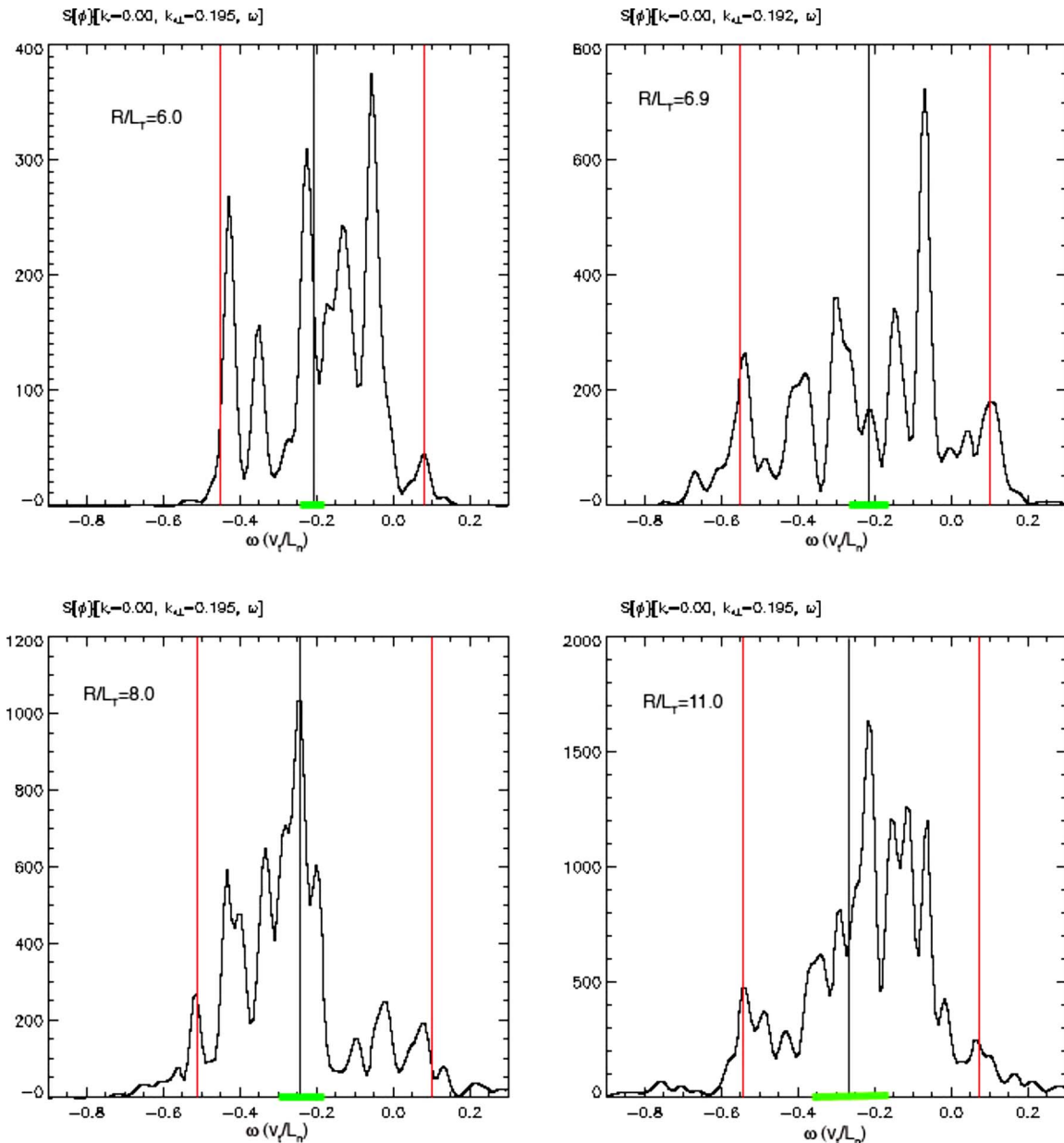
FIG. 5. (Color online) Frequency spectra for an L_T scan. The central vertical lines represent the ITG frequency, the outlying vertical lines show the width of the spectrum taken for Fig. 6, and the horizontal bar on the axis represents the linear growth rate. In all instances the frequency spectra are much wider than the linear growth rate. In addition, the widths of the spectra remain similar throughout the scan in spite of an increase in the growth rate by a factor of 3. The spread in damped mode frequencies varies little with L_T and closely matches the width of the nonlinear spectra as seen in Fig. 6.

ther the linear growth rate or the zonal flow velocity.

It should be noted that GLF23 parameter scans show that the spread in linear mode frequencies is only weakly dependent on gradient scale lengths and safety factor but strongly dependent on magnetic shear s. The frequency spread is much narrower for low values of s. However, this behavior is not observed in the nonlinear spectrum of GYRO simulations which still show wide spectra similar to higher s spectra. If the low s nonlinear spectrum is to be interpreted in terms of available linear eigenmodes, one must assume that there are important eigenmodes at low s that are not captured by GLF23's eight-field fluid closure or that GLF23 does not capture the correct shear dependence of the damped eigenmode frequencies.

B. Transport fluxes

Excitation of damped eigenmodes generally causes a reduction in transport fluxes. Their effect on energy balance and transport can roughly be conceptualized as the opposite of an instability, i.e., they dissipate energy from the fluctuations, allowing gradients to steepen. In order to illustrate the effect of damped eigenmodes on heat flux, we write the electrostatic potential and pressure fluctuations as a superposition of six modes corresponding to the six modes defined by GLF23,

$$\phi = \beta_1 + \beta_2 + \beta_3 + \beta_4 + \beta_5 + \beta_6, \tag{5}$$

$$p = R_1\beta_1 + R_2\beta_2 + R_3\beta_3 + R_4\beta_4 + R_5\beta_5 + R_6\beta_6. \tag{6}$$
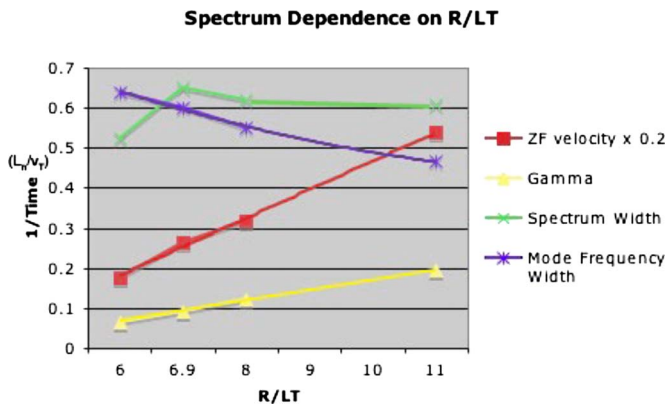
FIG. 6. (Color online) Plot of the width of the nonlinear frequency spectrum (as shown by the vertical lines in Fig. 5) at $k_x=0$, $k_y=.2$ in comparison with other quantities that might determine the width of the spectrum. The linear growth rate and the zonal flow velocity increase significantly over the L_T scan. However, the widths of the nonlinear spectra vary little and are matched closely by the spread in eigenmode frequencies.

The heat flux component at wavenumber k is proportional to the $\phi^* p$ cross correlation,

$$Q(k) = k_y \, \mathrm{Im}[\phi(k)^* p(k)]. \tag{7}$$

The R_i are complex coefficients defining the correct $\phi^* p$ cross phases for each eigenmode. The heat flux can also be expressed in the eigenmode basis as

$$Q(k) = k_y \, \mathrm{Im}\left(\sum_i R_i \beta_i^2 + \sum_{i,j \neq i} R_i \beta_i \beta_j^* \right). \tag{8}$$

The β_i^2 are positive definite so the direction of the flux contribution from these terms depends only on the coefficients $\mathrm{Im}(R_i)$. The contribution of cross terms is more difficult to characterize. This is the topic of the current study with the reduced three-field ITG model, where it appears that (with some interesting exceptions) these terms largely cancel out so that the flux is dominated by the β_i^2 terms. Damped mode phase data are available from GLF23 and indicate that

three of the five damped modes would give an inward contribution to heat flux. The unstable mode gives an outward component of flux, as do the two most weakly damped modes, albeit at a significantly reduced level in comparison to the unstable mode. As a result, damped mode excitation causes a net reduction in heat flux in comparison with the transport that would result solely from the instability.

In order to estimate the magnitude of the effect of damped eigenmodes on transport, comparisons are made between the quasilinear flux and the true flux. Quasilinear theory estimates fluxes assuming that the dynamics are governed solely by the unstable mode. A quasilinear flux is constructed by multiplying the ϕ^2 intensity from a nonlinear simulation by the linear response function from a linear simulation, as represented by Eq. (9). For an initial value code, a linear simulation can only identify the fastest growing mode so all quantities (phases, frequencies, etc.) derived from the data are associated with the instability. As a result, this procedure amounts to replacing p in the heat flux expression with the estimate $p = R_1 \phi$ which is accurate only if the fluctuations lie almost exclusively on the unstable manifold. This amounts to keeping only the $R_1 \beta_1^2$ term in Eq. (8),

$$Q_{ql}(k) = k_y \, \mathrm{Im}[R_1(k)\phi^2(k)]. \tag{9}$$

In order to construct a quasilinear flux, the response function R_1 is taken from a linear GS2 (Ref. 31) run and is used in conjunction with data from a nonlinear GYRO simulation. GS2 is capable of initializing a linear simulation for a range of radial wavenumbers, whereas GYRO is limited to $k_x=0$ for linear simulations. The response function is plotted in Fig. 7. Using data from these two codes should not be a problem, as GS2 and GYRO have been extensively benchmarked for CYCLONE-base case parameters. Comparisons between GS2 and GYRO were made for $k_x=0$ wavenumbers and the quasilinear fluxes agree to within 2%.

The quasilinear flux is a good estimate of the true flux in the linear phase before nonlinear energy transfer excites damped eigenmodes. This corresponds to $t < 80 L_T / v_T$ in Fig.
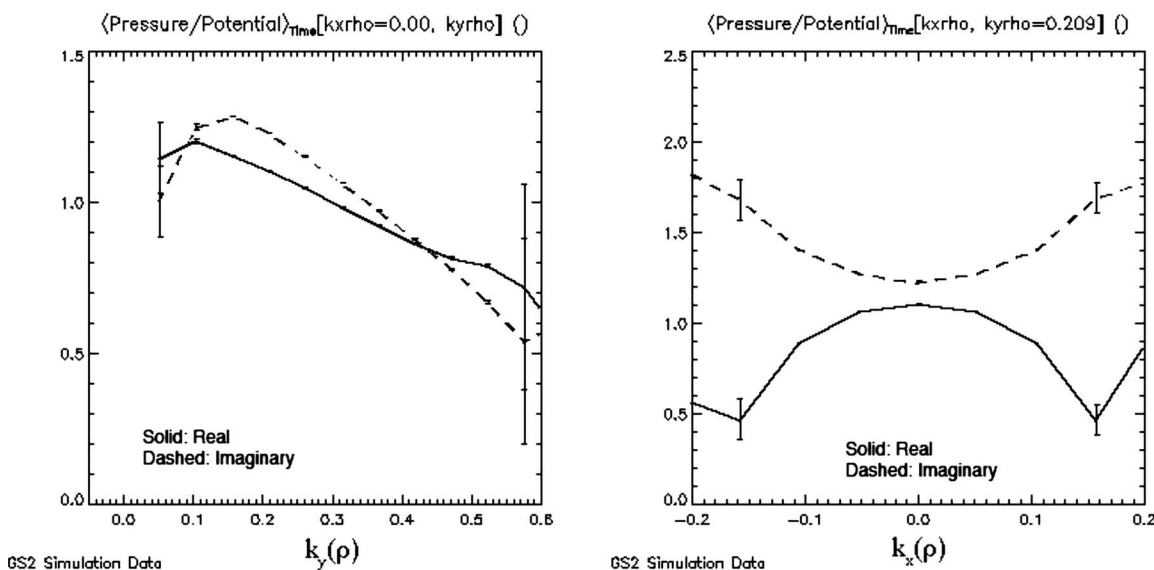
FIG. 7. The linear response function P/ϕ from linear GS2 data for $k_x=0$ as a function of k_y (left) and $k_y=0.2$ as a function of k_x right.

Total Heat Flux - Early Time

Black: quasilinear flux
Red: true flux
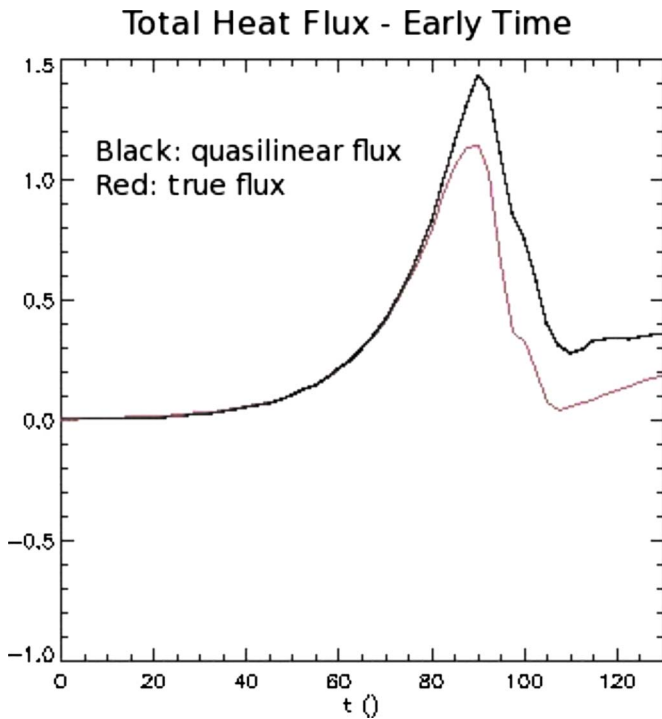
FIG. 8. (Color online) A comparison of the quasilinear and true fluxes during the linear growth phase and the transition from the linear to nonlinear regime. At early times, the two fluxes are identical but diverge when nonlinear energy transfer excites damped eigenmodes.

8, which shows the two fluxes as functions of time starting from infinitesimal initial conditions. In the saturated state, the quasilinear flux consistently overestimates the true flux as would be expected when damped eigenmodes are excited. This is seen in Fig. 8 after $t \approx 80 L_T / v_T$ and in a longer time history of the two fluxes in Fig. 9. The ratio of total true flux to quasilinear flux is, on average, 0.64. At $k_x = 0$, the ratio is 0.79 and the quasilinear estimate grows increasingly poor as k_x increases, as seen in Fig. 10.

These comparisons indicate that damped eigenmodes have an effect of approximately 36% on transport fluxes. It is important to note that this comparison provides an estimate of the impact of damped eigenmodes on transport fluxes, but

Total Heat Flux

Black: quasilinear flux
Red: true flux
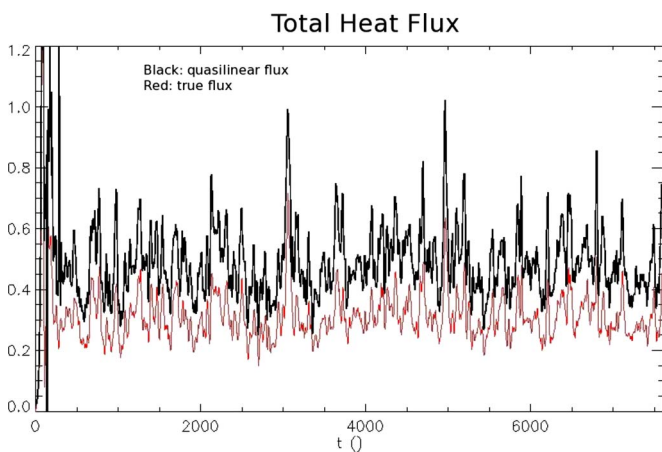
FIG. 9. (Color online) A long time history of the quasilinear and true heat fluxes. On average, the true flux is 64% of the quasilinear flux.

the impact on energy balance and saturation could be much larger as damped modes can provide an energy sink at all wavenumbers including $k_y = 0$, whereas only fluctuations at finite k_y affect transport.

C. Phase pdfs

The eigenvector of a linear eigenmode defines cross-phase relations between fields. Nonlinear cross phases in saturated turbulence are the result of the interaction between all excited eigenmodes. Heat flux is expressed in terms of the cross phase between electrostatic potential and pressure fluctuations, and so is dependent on the eigenmodes that make up the fluctuations, as discussed in the previous section. We examine pdfs of phase angles $\tan^{-1}[\mathrm{Im}(p^*\phi)/\mathrm{Re}(p^*\phi)]$ to better understand the behavior of nonlinear cross phases and their relation to damped eigenmode excitation.

A phase angle pdf is constructed by tracking (for different wavenumbers) the number of instances in time when the phase angle falls in different angular ranges. In addition, the pdf can be intensity weighted, amplifying the probability by a factor proportional to the instantaneous intensity, ϕ^2. This serves to highlight regions (in time and k space) that are important for transport and makes phase pdfs smoother. However, it is unclear what information is eliminated during this process. For instance, if damped eigenmode excitation is associated with periods of low intensity, then intensity weighting acts to filter out the damped eigenmode contribution to phase angle dynamics. We consider both weighted and unweighted phase angle pdfs in this paper. Intensity weighted pdfs are examined in Ref. 22 where nonlinear phase pdfs are compared to the linear phase angles of the unstable mode for CTEM turbulence. There is a close correspondence between linear and nonlinear phase angles. In this work, a correspondence is also observed between phase pdfs and linear mode phase angles. However, the peak of the pdf about the linear phase angle is broadened. While the width is smaller than the spread $\Delta\omega$ of the frequency spectrum, we will show that it is consistent with the excitation of other modes.

A long time simulation [2800 time steps corresponding to $t(v_T/L_T) = 500 - 7500$] was used to create phase angle pdfs. The intensity weighted phase pdf at $k_x = 0$ as a function of k_y is shown in Fig. 11(a). It is observed that the phase pdf is peaked near the phase angle of the most unstable mode for most wavenumbers. The exception is $k_y = 0.05$ where there is a secondary peak that aligns with the linear phase angle and a larger peak which is offset from the linear angle, as seen in Fig. 11(b). The larger peak may correspond to another mode or it may reflect the net effect of multiple interacting modes. Figure 12 shows two unweighted phase pdfs that are representative of most phase pdfs. The phase pdfs have widths that range from roughly 0.5 to 1.5 rad and also exhibit non-Gaussian "tails" and "bumps." While there is little in the literature regarding phase pdfs, it is plausible that many of these features are signatures of multiple mode excitation. Linear theory defines a single phase angle for each eigenmode, not a peaked distribution of phase angles.

For nonlinear data, one would expect some nonlinear
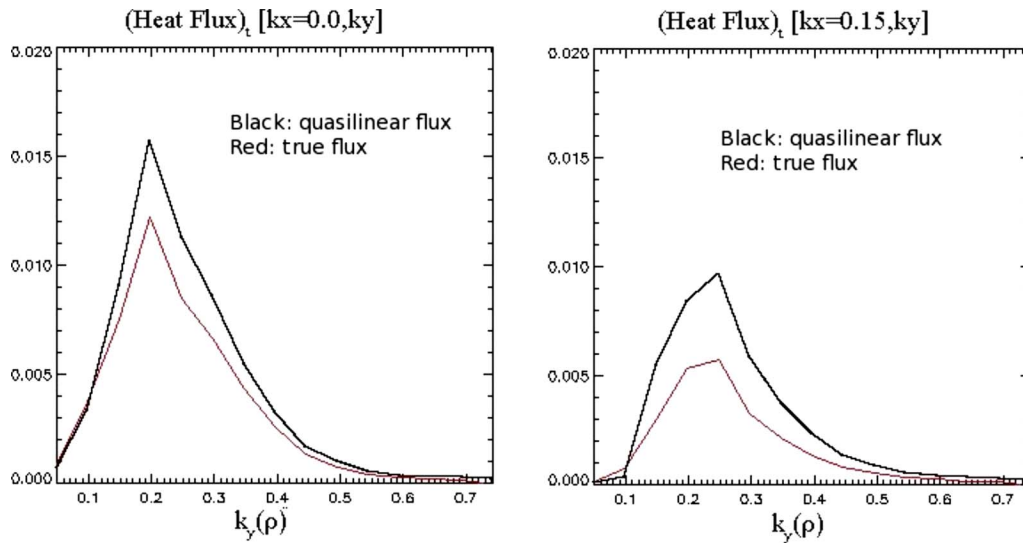
FIG. 10. (Color online) A comparison of the quasilinear and true fluxes at $k_x=0$ as a function of k_y (left) and $k_x=0.15$ as a function of k_y (right). The quasilinear approximation worsens as k_x increases.

broadening but it is unclear how large this effect would be. A phase pdf with a finite width can be easily explained by the interaction of multiple modes. Consider the interaction between a dominant mode ϕ_1 and another mode ϕ_2 with smaller amplitude and different phase angle and frequency as modeled by

$$\phi = \phi_1 e^{-i\omega_1 t} + \phi_2 e^{-i\omega_2 t}, \tag{10}$$

$$p = \phi_1 e^{-i\alpha_1} e^{-i\omega_1 t} + \phi_2 e^{-i\alpha_2} e^{-i\omega_2 t}. \tag{11}$$

The dominant and subdominant mode phase angles/frequencies are represented by α_1 and α_2/ ω_1 and ω_2, respectively. Taking ϕ_2/ϕ_1 as a small parameter, the phase angle, $\tan^{-1}[\text{Im}(p^*\phi)/\text{Re}(p^*\phi)]$ can be expanded to first order in ϕ_2/ϕ_1,

$$\alpha_{\text{nl}} = \alpha_1 + \frac{\phi_2}{\phi_1} \frac{\tan(\alpha_1)}{1 + \tan^2(\alpha_1)} A[\alpha_1, \alpha_2, (\omega_1 - \omega_2)t], \tag{12}$$

$$A[\alpha_1, \alpha_2, (\omega_1 - \omega_2)t]$$
$$= \frac{\sin[\alpha_1 + (\omega_1 - \omega_2)t] + \sin[\alpha_2 + (\omega_2 - \omega_1)t]}{\sin(\alpha_1)}$$
$$- \frac{\cos[\alpha_1 + (\omega_1 - \omega_2)t] + \cos[\alpha_2 + (\omega_2 - \omega_1)t]}{\cos(\alpha_1)}. \tag{13}$$

The nonlinear phase angle has a constant term (α_1) and a smaller amplitude term (proportional to ϕ_2/ϕ_1) oscillating at the beat frequency. This would manifest itself in a phase pdf
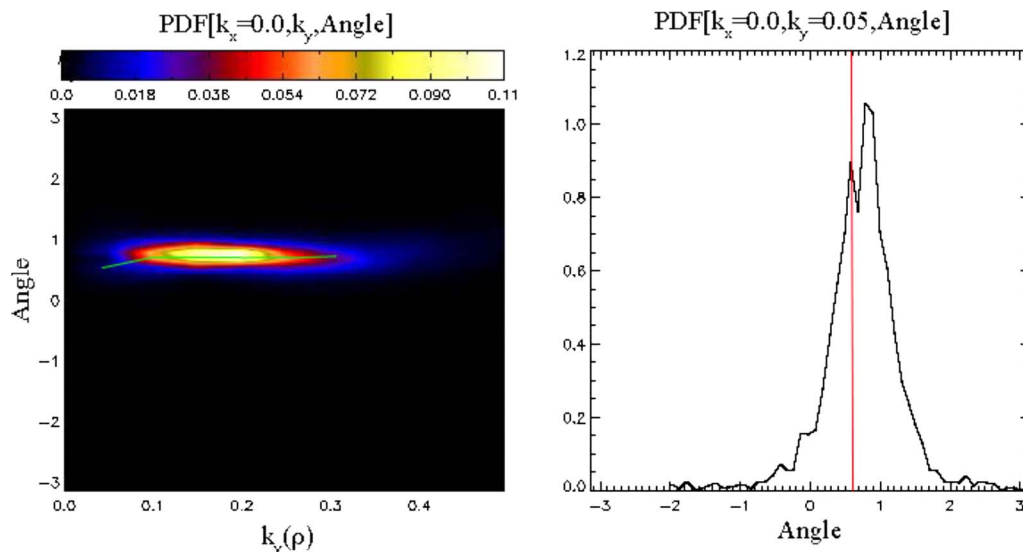
FIG. 11. (Color online) Left: Intensity weighted phase pdf at $k_x=0$ as a function of k_y. The line represents the linear phase angle. Right: Unweighted phase pdf for the wavenumber $k_x=0$, $k_y=.05$. The vertical line represents the most unstable mode phase angle, which corresponds to a secondary peak in the phase pdf.
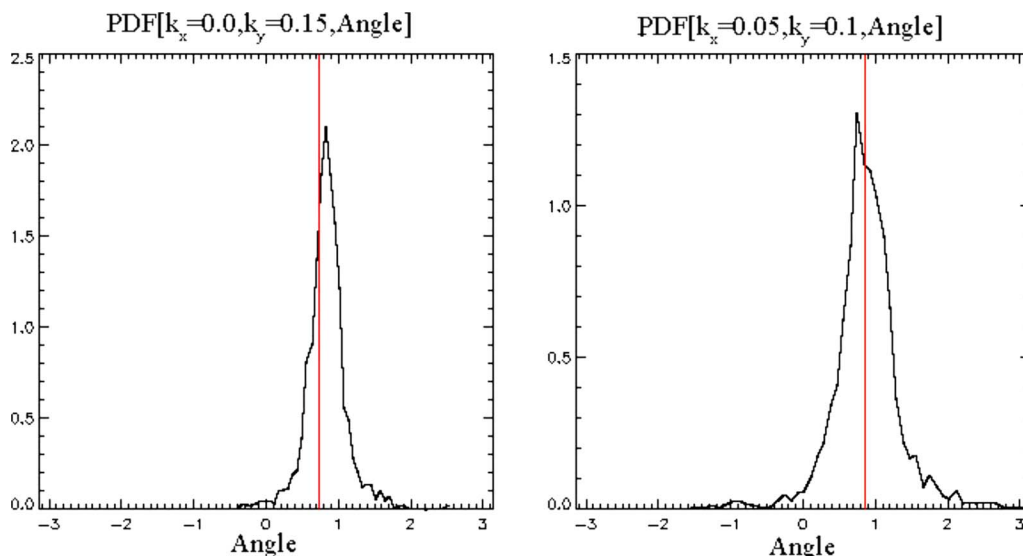
FIG. 12. (Color online) Unweighted phase angle pdfs for $k_x=0.05$, $k_y=0.1$ (left) and $k_x=0$, $k_y=0.15$ (right). The vertical lines represent the most unstable mode phase angle. These phase pdfs are representative of many wavenumbers that exhibit widths ranging from 0.5 to 1.5 rad and non-Gaussian tails and bumps.

as a peak at the dominant phase angle with a width proportional to the ratio of the mode amplitudes. This analysis applied to more than two modes would produce a similar result, i.e., a pdf peaked at the dominant phase angle with a width dependent on the relative mode amplitudes.

In order to develop more intuition regarding the structure of phase angle pdfs, a simple modeling exercise was undertaken. Heuristic signals for the electrostatic potential and pressure were created to model the interaction of multiple modes in creating a nonlinear phase angle. The electrostatic potential is modeled by taking the electrostatic potential signal from a long time simulation for a single wavenumber ($k_x=0$, $k_y=0.15$) near the peak of the spectrum in a nonlinear GYRO simulation. This signal is divided into six sections representing six linear eigenmodes,

$$\phi = \beta_1 + \eta(\beta_2 + \beta_3 + \beta_4 + \beta_5 + \beta_6), \qquad (14)$$

$$p = R_1\beta_1 + \eta(R_2\beta_2 + R_3\beta_3 + R_4\beta_4 + R_5\beta_5 + R_6\beta_6). \qquad (15)$$

As in Eq. (5), β_1 represents the unstable eigenmode and the remaining β_i represent the damped eigenmodes. Each β_i is modeled by a time segment of the long time simulation data. The damped eigenmodes are reduced in amplitude by the factor η. The pressure signal is created by multiplying the same mode signals (β_i) by complex constants (R_i), which give them the correct phase angles (as calculated by GLF23) for the different modes [Eq. (15)]. A net phase angle is determined from these heuristic pressure and potential signals and a phase pdf is calculated. It is observed that the phase pdf is peaked near the unstable mode phase angle for a wide range of η. As η is increased, the phase pdf broadens and other features (secondary peaks, bumps, and tails) become more prominent. For each value of η, an energy ratio can be calculated $[\eta^2(\Sigma_{i=2,6}\gamma_i)/\gamma_1]$. This energy ratio is the ratio of the rate of energy dissipation (due to the damped modes) to the energy input rate (from the instability). The model phase pdfs most closely match the true nonlinear pdf when the

energy ratio is between 0.20 and 0.44, i.e., the damped modes are dissipating roughly 30% of the energy input by the instability. This is consistent with the magnitude of the effect of damped eigenmodes on transport fluxes as estimated in the previous section.

IV. FLUCTUATIONS AT ZONAL WAVENUMBERS

Fluctuations at zonal wavenumbers ($k_y=0$) are known to be closely tied to saturation of ITG turbulence. It is often stated that the dominant saturation mechanism is the shearing of turbulent eddies to high radial wavenumber by zonal flows. However, the shearing rate due to self-consistent zonal flows is not likely to be high enough to account for the drastic reduction in fluctuation levels associated with coupling to zonal modes.[15–17] It is important to distinguish between zonal flows [Rosenbluth and Hinton (RH)] and other zonal fluctuations. RH zonal flows are $\omega=0$, $k_y=0$ fluctuations which are linearly undamped in the absence of collisions. There are other zonal modes which *are* linearly damped. The best known of these is the GAM which has a relatively high frequency and is linearly damped. The GAM is easily identified in the nonlinear frequency spectrum. In addition to the GAM, there are other eigenmodes with low but finite frequency identified in both experiment[32] and analytical treatments.[9,33]

Multiple zonal eigenmodes can be derived from both kinetic theory and fluid theory. Gao presented a series of damped zonal eigenmodes including the standard GAM and a low frequency GAM. An infinite number of linear modes can be derived from the gyrokinetic equation and it is plausible that other low to zero frequency damped eigenmodes exist which have not been identified or cataloged. The eigenmode solver in GLF23 identifies six damped eigenmodes at $k_y=0$. Two have low but finite frequencies and four others have exactly zero real frequencies. There is reason to be wary of the results of gyro-Landau fluid equations for zonal

Spectrum$\{\phi\}[k_x=0.1, k_y=0.0, \omega]$
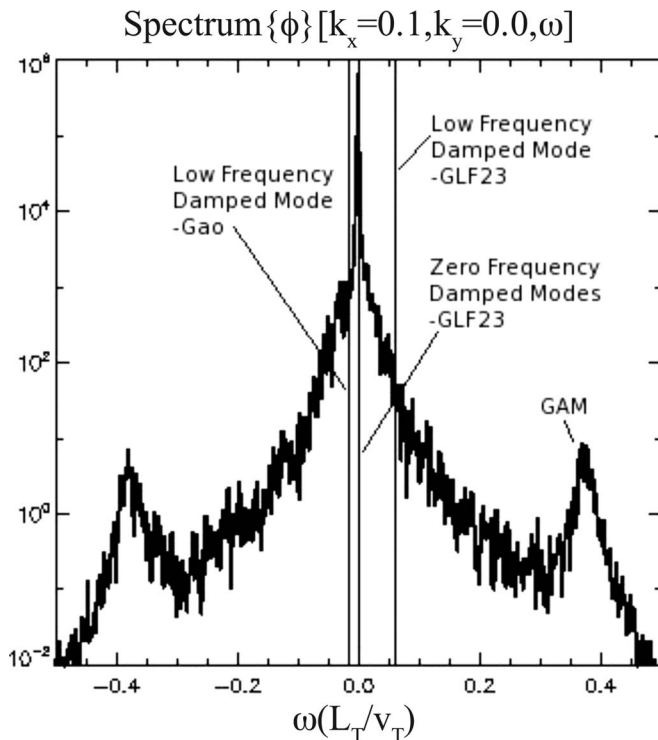
FIG. 13. Nonlinear frequency spectrum for $k_y=0$, $k_x=0.1$. The vertical lines represent known low frequency damped eigenmodes whose damping rates are comparable to the maximum ITG growth rate.

modes[11] but it is important to note that gyro-Landau fluid equations indicate a series of low to zero frequency zonal eigenmodes rather than a single zero frequency undamped mode.

At finite k_y, damped eigenmodes at zonal wavenumbers can only be excited by nonlinear energy transfer. It has been shown that energy transfer to zonal wavenumbers is the favored nonlinear transfer channel.[4,34] As a result, the intensity spectrum is dominated by zonal intensity. The amount of intensity in zonal wavenumbers is large enough that even if only a portion of the zonal energy is in linearly damped zonal modes (as opposed to the undamped RH zonal flows), these damped eigenmodes could be the dominant energy sink. This would be consistent with the observed intimate connection between zonal mode excitation and saturation while resolving the problem of the inadequate shearing rate produced by self-consistent zonal flows.

In spite of the drawbacks of these mode derivations (Gao used a different parameter regime and for GLF23 there are questions about the closure at $k_y=0$), it is instructive to make some qualitative comparisons of the mode frequencies with the nonlinear frequency spectrum at $k_y=0$. The nonlinear frequency spectrum at $k_y=0$ is characterized by a sharp peak at zero frequency and a secondary peak at the GAM frequency. Although the spectrum is sharply peaked at $\omega=0$, there is a finite width to the spectrum with significant intensity extending off axis. Both the low frequency Gao mode and to a lesser extent the finite frequency GLF23 modes are in ranges of significant intensity in the nonlinear frequency spectrum as shown in Fig. 13. The damping rates of these modes are on the same order of magnitude as the peak ITG growth rate

γ_{ITG}. If these (and/or other similar) modes make up part of the zonal fluctuations, then these low frequency damped modes are potentially a potent energy sink. Using $U=p^2 +(1+k^2)\phi$ as an approximate surrogate for a conserved gyrokinetic fluctuation energy, some rough energy balance estimates can be made. In saturation, zonal fluctuations account for 56% of the total fluctuation energy. For a rough estimate of energy balance it is reasonable to assume that the damping rate of a zonal damped eigenmode is comparable to the peak growth rate of the instability. In addition, we make a conservative estimate that 70% of the nonzonal energy is on the unstable manifold in regions of instability. The remaining 30% is subject to either high-k damping (intrinsic or numerical) or damping due to damped eigenmode excitation in the region of instability. We assume that the finite k_y damping rates are also on the order of γ_{ITG}. Energy balance can then be written

$$0.7\gamma_{ITG}U_{dw} - 0.3\gamma_{ITG}U_{dw} - \gamma_{ITG}\eta U_{zm}$$
$$= 0.7\gamma_{ITG}U_{dw} - 0.3\gamma_{ITG}U_{dw} - \gamma_{ITG}\eta 1.3 U_{dw}$$
$$= 0,$$

where U_{dw} is the drift wave (nonzonal) fluctuation energy, U_{zm} is the zonal fluctuation energy, and η is the percentage of the zonal fluctuation energy associated with damped zonal modes. With these estimates, energy balance is achieved for $\eta=0.15$, i.e., only 15% of the zonal fluctuations must be low frequency damped modes in order to account for saturation. Although we have made very coarse estimates, it is clear that only a portion of the zonal fluctuations must be linearly damped in order for this to be a very significant energy sink.

The nonlinear cross phase of $p^*\phi$ at $k_y=0$ shows a strong signature of multiple mode behavior. In Fig. 14, the phase pdf is peaked near $\pm\pi$, the phase angle of the standard RH zonal flow. In addition, there is significant probability in the entire angular domain. The cause of this broad pdf is made apparent by observing the temporal behavior of the phase angle as is seen in Fig. 15. For periods of time, the phase angle fixes at $\pm\pi$ but in other periods, it rotates slowly in time. There is a striking resemblance between this phase angle behavior and the behavior observed in the reduced ITG model where there are three competing modes with comparable amplitudes.[3] For these parameters ($q=1.4$) the standard GAM amplitude is small enough that it is unlikely to cause such a large change in phase angle dynamics. To verify this, a digital filter was used to decrease the GAM contribution and the resulting change in phase angle behavior was barely discernible. It is likely that two or more low frequency zonal modes are competing at $k_y=0$ and the time scale of phase rotation is related to the beat frequencies of these modes. More recent results, while not ruling out the possibility of zonal modes providing a direct energy sink, indicate that their most important role may be in coupling to damped eigenmodes at finite k_y.

We have recently become aware of concurrent work[28] that suggests that zonal wavenumbers do not provide a large energy sink for a mixed ITG/TEM GYRO simulation. In that work, diagnostics for nonlinear transfer of conserved entropy (or turbulent energy) indicate that energy is not preferentially

PDF[k_x,k_y=0.0,Angle]
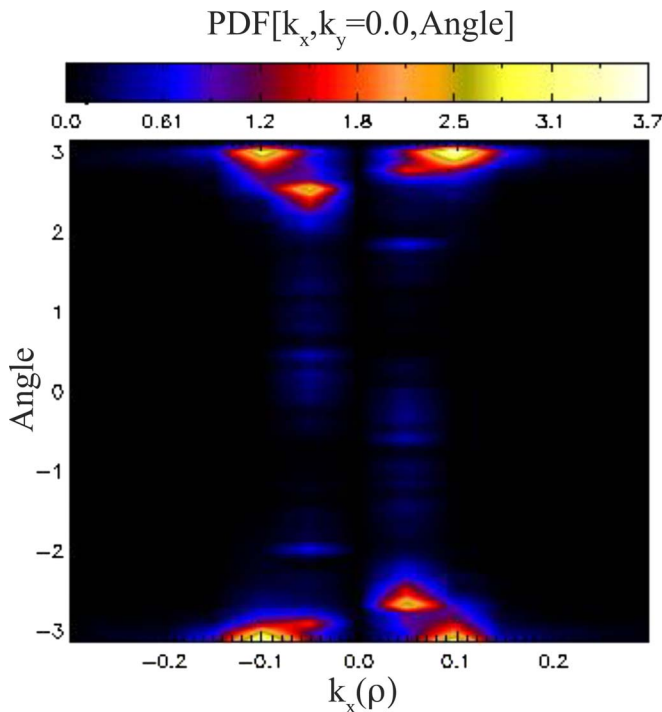
FIG. 14. (Color online) $p^*\phi$ phase angle pdf for $k_y=0$. The pdf at $k_x=0.05$ shows significant probability over the entire range of angles.

transferred to zonal modes but rather uniformly transferred to all stable wavenumbers. That work also concludes that "turning off Landau damping" has little effect on saturation levels. These conclusions and the diagnostics leading to them merit further scrutiny. We foresee developing and implementing a gyrokinetic diagnostic like that described above in Sec. II that directly measures the rate at which energy from the background is injected into or removed from fluctuations at finite amplitude. With such diagnostics the extent to which damped eigenmodes at zonal wavenumbers provide a sink to fluctuation energy can be determined directly.
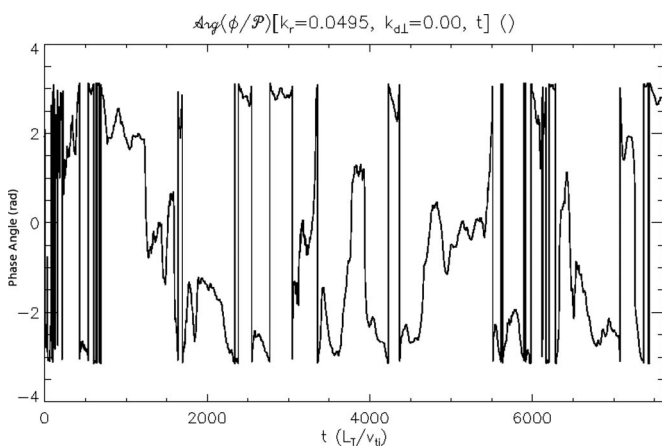
FIG. 15. Time history of the phase angle for wavenumber $k_y=0$, $k_x=.05$. The phase angle fixes temporarily at $\pm\pi$ but also rotates for long periods of time, indicating the interaction of multiple eigenmodes. Digitally filtering out the high frequency GAM contribution does not significantly change the phase angle dynamics suggesting that the important interacting modes are not GAMs but low frequency modes.

V. SUMMARY AND CONCLUSIONS

We have presented results from gyrokinetic simulations of ITG turbulence, which suggest that multiple stable eigenmodes are excited nonlinearly to amplitudes sufficient to significantly impact saturation and transport. Current gyrokinetic codes are initial value codes and thus are unable to provide direct information about anything more than the most unstable mode. As a result, we have applied less direct tests to gyrokinetic simulation data to identify signatures of multiple eigenmode behavior. These tests fall into three categories: (1) frequency spectra, (2) comparisons of quasilinear and nonlinear fluxes, and (3) phase relations. The gyro-Landau fluid model from GLF23 was used to solve for frequency and phase information for multiple modes and these data were used in conjunction with GYRO simulation data in applying these tests. The results are summarized as follows.

For fluctuations at $k_y \neq 0$, we have the following:

(1) Frequency spectra: The width of the nonlinear frequency spectrum tracks the spread in damped mode frequencies (as given by GLF23) very closely. Both the nonlinear spectrum and the damped mode frequencies spread as k_y increases. In addition, frequency spectra are found to be much wider than what would be expected simply from nonlinear broadening about the frequency of the most unstable eigenmode. In saturation this width should be of the order of the linear growth rate if damped eigenmodes are not excited. Scans in L_T indicate that the width of the spectrum does not scale with the linear growth rate or zonal flow velocity (possible Doppler shift) but changes only slightly for a wide range of L_T. This is consistent with the spread in linear mode frequencies which is also only weakly sensitive to changes in L_T. We conclude that much of the intensity in the nonlinear frequency spectrum is a manifestation of damped eigenmode excitation.

(2) Transport fluxes: Quasilinear estimates of transport fluxes implicitly assume that transport is determined solely by the most unstable mode. Stable eigenmodes generally reduce fluxes and often provide an inward contribution to fluxes. It was found that quasilinear fluxes consistently overestimate the true nonlinear flux. At $k_x=0$ the true flux is 79% of the quasilinear flux and the quasilinear estimate worsens as k_x increases, so that the total flux is 64% of the total quasilinear flux. This gives an estimate of the magnitude of the effect of damped eigenmodes with $k_y \neq 0$.

(3) Phase relations: Linear eigenmodes are associated with characteristic phase relations. It was found that phase angle pdfs are peaked near the unstable mode phase angle and have a finite width and non-Gaussian features (bumps and tails) that indicate multiple mode behavior. A simple model was used to demonstrate how a dominant mode would interact with smaller amplitude modes to create a phase pdf centered at the dominant mode phase angle with a width proportional to the relative amplitudes of the modes. It was shown that the phase pdf at the wavenumber at the peak of the intensity spectrum has a width that is consistent with a damped mode

effect of roughly 30%. This is consistent with the quasilinear flux estimate.

For fluctuations at $k_y=0$, we presented $p^*\phi$ cross-phase data that indicate the excitation of multiple eigenmodes at zonal wavenumbers. The phase angle pdf is peaked at the phase angle of the RH zonal flow but also shows significant probability in the entire angular range. The cross-phase angle is fixed at $\pm\pi$ for periods of time but intermittently transitions to rotating behavior for long periods of time. This behavior remains even when the high frequency GAM contribution is digitally filtered out of the spectrum, suggesting that zonal fluctuations are a superposition of the standard zonal flow with one or more other zonal modes. We discussed known damped zonal modes whose frequencies are consistent with the zonal frequency spectrum and whose damping rates make them excellent candidates for being the dominant energy sink of ITG turbulence. Rough energy balance estimates demonstrate that only a small part of the zonal fluctuations need to be damped in order for this to be a significant energy sink. In addition, recent results indicate the possibility that zonal modes may be instrumental in exciting damped eigenmodes at nonzonal wavenumbers.

In conclusion, while the tests we have applied to gyrokinetic simulation data have been, of necessity, somewhat indirect, the results tell a consistent story regarding damped eigenmode excitation. Consideration of frequency spectra, phase behavior, and quasilinear flux estimates all indicate that damped eigenmodes are important in saturation and transport for ITG turbulence. The combined weight of these tests lends credence to the claim that damped eigenmodes are crucial to a complete understanding of microturbulence.

It is important to note that we have exclusively considered CYCLONE-base case ITG turbulence. It is likely that there are other parameter regimes for ITG turbulence in addition to turbulence driven by other instabilities for which damped eigenmodes are even more important to the dynamics. Results from fluid models indicate that damped eigenmodes are critical in CTEM turbulence where saturation is tied to zonal density fluctuations. It is plausible that finite k_y damped eigenmodes are the primary energy sink for ETG turbulence since zonal flows are less important than in ITG turbulence.

The deleterious effect of turbulent transport on plasma confinement is the primary reason for studying microturbulence. We estimate that damped eigenmodes cause roughly a 35% reduction in transport fluxes. An effect of this magnitude should be understood and added to the concepts that researchers use to inform their intuition regarding turbulent transport. In addition, while there is no reason to assume that existing codes fail to resolve important damped eigenmodes, this should be verified and taken into consideration when performing simulations.

The method by which saturation is achieved is a crucial aspect of instability-driven turbulence. The effect of damped eigenmodes on saturation is possibly much larger than the effect on transport since, in addition to the dissipation at finite k_y, damped zonal eigenmodes have the potential to be the dominant energy sink. It is clear that zonal fluctuations are tied to the saturation of ITG turbulence. Zonal flows cause shearing of drift waves and energy transfer to high k_x, but this effect is not large unless shearing rates are considerably larger than the turbulent correlation rate. We suggest the possibility of a different paradigm for how zonal fluctuations could affect saturation. Zonal fluctuations are a superposition of multiple eigenmodes—the weakly damped RH zonal flow and other low frequency linearly damped zonal modes that are the primary energy sink.

ACKNOWLEDGMENTS

[1] See Table 1 in A. J. Brizard and T. S. Hahm, Rev. Mod. Phys. **79**, 421 (2007), showing saturation theories for a variety of instabilities. None invoke damped eigenmodes as a direct sink of energy.

[2] D. A. Baver, P. W. Terry, R. Gatto, and E. Fernandez, Phys. Plasmas **9**, 3318 (2002).

[3] P. W. Terry, D. A. Baver, and S. Gupta, Phys. Plasmas **13**, 022307 (2006).

[4] R. Gatto, P. W. Terry, and D. A. Baver, Phys. Plasmas **13**, 022306 (2006).

[5] P. W. Terry and R. Gatto, Phys. Plasmas **13**, 062309 (2006).

[6] P. W. Terry, D. R. Hatch, and J.-H. Kim, Bull. Am. Phys. Soc. **53**, 108 (2008).

[7] Z. Lin, T. S. Hahm, W. W. Lee, W. M. Tang, and R. B. White, Science **281**, 1835 (1998).

[8] N. Winsor, J. L. Johnson, and J. M. Dawson, Phys. Fluids **11**, 2448 (1968).

[9] Z. Gao, K. Itoh, H. Sanuki, and J. Q. Dong, Phys. Plasmas **13**, 100702 (2006).

[10] P. H. Diamond, S.-I. Itoh, K. Itoh, and T. S. Hahm, Plasma Phys. Controlled Fusion **47**, R35 (2005).

[11] M. N. Rosenbluth and F. Hinton, Phys. Rev. Lett. **80**, 724 (1998).

[12] Z. Lin, T. S. Hahm, W. W. Lee, W. M. Tang, and P. H. Diamond, Phys. Rev. Lett. **83**, 3645 (1999).

[13] R. E. Waltz, R. L. Dewar, and X. Garbet, Phys. Plasmas **5**, 1784 (1998).

[14] H. Biglari, P. H. Diamond, and P. W. Terry, Phys. Fluids B **2**, 1 (1990).

[15] W. M. Nevins, J. Candy, S. Cowley, T. Dannert, A. Dimits, W. Dorland, C. Estrada-Mila, G. W. Hammett, F. Jenko, M. J. Pueschel, and D. E. Shumaker, Phys. Plasmas **13**, 122306 (2006).

[16] G. R. McKee, R. J. Fonck, M. Jakubowski, K. H. Burrell, K. Hallatschek, R. A. Moyer, W. Nevins, D. L. Rudakov, and X. Xu, Plasma Phys. Controlled Fusion **45**, A477 (2003).

[17] Y. Z. Zhang and S. M. Majahan, Phys. Fluids B **4**, 1385 (1992).

[18] T. S. Hahm, M. A. Beer, Z. Lin, G. W. Hammett, W. W. Lee, and W. M. Tang, Phys. Plasmas **6**, 922 (1999).

[19] P. W. Terry and D. A. Baver, Phys. Rev. Lett. **89**, 205001 (2002).

[20] P. W. Terry, Phys. Rev. Lett. **93**, 235004 (2004).

[21] J. Candy and R. E. Waltz, J. Comput. Phys. **186**, 545 (2003).

[22] T. Dannert and F. Jenko, Phys. Plasmas **12**, 072309 (2005).

[23] F. Jenko, W. Dorland, M. Kotschenreuther, and B. N. Rogers, Phys. Plasmas **7**, 1904 (2000).

[24] M. Kammerer, F. Merz, and F. Jenko, Phys. Plasmas **15**, 052102 (2008).

[25] R. E. Waltz, G. M. Staebler, W. Dorland, G. W. Hammett, and M. Kotschenreuther, Phys. Plasmas **4**, 2482 (1997).

[26] A. M. Dimits, G. Bateman, M. A. Beer, B. I. Cohen, W. Dorland, G. W. Hammett, C. Kim, J. E. Kinsey, M. Kotschenreuther, A. H. Kritz, L. L. Lao, J. Mandrekas, W. M. Nevins, S. E. Parker, A. J. Redd, D. E. Shumaker, R. Sydora, and J. Weiland, Phys. Plasmas **7**, 969 (2000).

[27] G. S. Lee and P. H. Diamond, Phys. Fluids **29**, 3291 (1986).

[28] R. E. Waltz and C. Holland, Phys. Plasmas **15**, 122503 (2008).

[29] J. E. Kinsey, G. M. Staebler, and R. E. Waltz, Phys. Plasmas **12**, 052503 (2005).

[30] N. Mattor and P. W. Terry, Phys. Fluids B **4**, 1126 (1992).

[31] W. Dorland, F. Jenko, M. Kotschenreuther, and B. N. Rogers, Phys. Rev. Lett. **85**, 5579 (2000).

[32] A. Fujisawa, A. Shimizu, H. Nakano, S. Ohsima, K. Itoh, H. Iguchi, K. Matsuoka, S. Okamura, S.-I. Itoh, and P. H. Diamond, Plasma Phys. Controlled Fusion **48**, A365 (2006).

[33] K. Itoh, S.-I. Itoh, P. H. Diamond, T. S. Hahm, A. Fujisawa, G. R. Tynan, M. Yagi, and Y. Nagashima, Phys. Plasmas **13**, 055502 (2006).

[34] C. Holland, P. H. Diamond, S. Champeaux, E. Kim, O. Gurcan, M. N. Rosenbluth, G. R. Tynan, N. Crocker, W. Nevins, and J. Candy, Nucl. Fusion **43**, 761 (2003).